Simulation of inflow turbulence noise

Thomas P. Lloyd[a,b*], Mathieu Gruber[c], Stephen R. Turnock[a] and Victor F. Humphrey[b]

[a]Fluid-Structure Interactions Research Group; [b]Institute of Sound and Vibration Research, University of Southampton, Southampton, UK. SO17 1BJ; [c]Department of Acoustic, Snecma Villaroche, Rond point rene Ravaud, REAU, 77550 Moissy-Cramayel, FRANCE.

1 Introduction

Broadband noise of turbomachines has become an important design consideration in numerous applications, including axial fans, marine propulsors and wind turbines. *Leading edge* (or *inflow turbulence*) noise has been shown to dominate when the flow into the rotor is turbulent (Carolus et al., 2007). In case of a submarine propeller, this occurs when the turbulent boundary layer of the hull enters the propulsor. For wind turbines, the inflow turbulence may be due to the atmospheric boundary layer or wakes from upstream turbines.

Amiet (1975) derived an analytical model showing that the far field acoustic pressure is proportional to the integral length scale ($\mathcal{L}$) and square of the turbulence intensity (I^2). As such, the measurement or specification of these quantities is important in the investigation of inflow turbulence (IT) noise. Measurements have also focussed on the leading edge noise of fixed aerofoils (e.g. see Devenport et al. (2010)). The inflow turbulence in most cases is generated using grids placed in the flow of wind tunnels, thus generating approximately homogeneous, isotropic turbulence.

This noise source can also be studied numerically using synthetic turbulence. Christophe et al. (2007) used such a method implemented inside FLUENT to simulate a jet impinging on an aerofoil. The low Reynolds number of $36,000$ allowed a large eddy simulation (LES) to be performed. Curle's analogy (Curle, 1955) is used to compute the low-frequency noise. Since the compact formulation of this method is only valid at lower frequencies (when the aerofoil chord $c << \lambda$), Amiet's model is used for the high frequency part of the spectrum to account for diffraction effects, with the *rms* velocities predicted by LES used as input to the model.

2 Simulation Details

2.1 Numerical method

In this study, we employ the Improved Delayed DES (IDDES) technique of Shur et al. (2008). The IDDES extension reformulates the length scale used to switch between the RANS and LES regions so as to resolve part of the boundary layer in the unsteady mode; it has been described as a form of wall modelled LES when inflow turbulence is present (Shur et al., 2008). For the simulation of inflow turbulence noise this seems a natural choice, since the unsteadiness seen by the wall will increase compared with DES due to the presence of eddies inside the boundary layer.

IDDES re-formulates both the DES length scale and grid filter definitions. The grid filter is given as

$$\Delta = min(max[C_w d_w, C_w h_{max}, h_{wn}], h_{max}) \tag{1}$$

where C_w is a constant, d_w the wall distance, $h_{max} = max(\Delta_x, \Delta_y, \Delta_z)$ and h_{wn} the wall-normal grid spacing. The DES length scale becomes

$$L_{IDDES} = f_B(1 + f_e)L_{RANS} + (1 - f_B)L_{LES} \tag{2}$$

where L_{LES} includes the DDES functions. A full description of the model functions f_B and f_e is given by Shur et al. (2008). Turbulence modelling is handled by the $k-\omega$ SST model, which has been shown to provide improved predictions of broadband noise sources over the Spalart-Allmaras turbulence model (Greschner et al., 2008).

The governing equations are solved using the open-source, finite-volume code OpenFOAM. The equations are discretised in their integral form, and solved on multi-block structured grids, using co-located variables. The solution method is based on the PISO algorithm and Rhie-Chow interpolation.

2.2 Case description

The simulations presented are based on measurements of leading edge noise of a NACA 65(12)10 aerofoil made by Gruber (2012) in the DARP open-jet aeroacoustic wind tunnel at the University of Southampton.

* *corresponding author's e-mail*: T.P.Lloyd@soton.ac.uk

Turbulence is generated inside the nozzle contraction using two grids, placed $50mm$ upstream of the nozzle exit. Results are presented for a jet velocity corresponding to a Mach number of ~ 0.06.

Two sets of measurements are used for validation. The first consists of hot-wire probe data, which is used to estimate the integral length scale and turbulence intensity of the inflow turbulence. A second set is made up of far field noise measurements at $1.22m$ of a NACA 65(12)10 aerofoil of $0.15m$ chord and $0.45m$ span, held in the flow by end plates attached to the nozzle. The chord-based Reynolds number is approximately 2.9×10^5. The co-ordinate system is depicted in Figure 1.

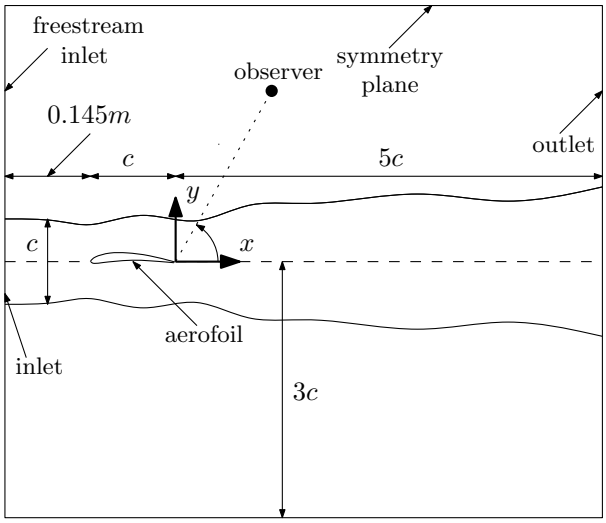

Figure 1: Schematic of simulation coordinate system and grid design.

2.3 Grid design

A structured gridding approach has been adopted. Grid design is influenced by the smallest size of eddy that can be resolved within the desired limit of computational expense. For the case considered here, the jet velocity, $U_\infty = 27.34ms^{-1}$, the mean streamwise turbulence intensity, $I = u'_{x,rms}/U_\infty$, is equal to 2.06% and the integral length scale is approximately $\mathcal{L} = 0.005m$. An ideal grid will contain cell sizes much smaller than the integral length scale; for example, Michel et al. (2009) recommend using 4 grid points per convection length scale $L_c = U_c/f$, where U_c is the convection velocity. We estimate the grid cutoff frequency, following Ask and Davidson (2006), to be $f_{max,i} = |u'_{i,rms}|/2\Delta_i$ where Δ_i is the grid spacing in the direction. Hence, the smallest cell size must be half the highest resolvable eddy length. The resulting grid has dimensions of $L_x \times L_y \times L_z = 7c \times 6c \times 0.1c$. To further reduce the number grid cells required, the nozzle walls are not included, with the jet exit placed at the simulation inlet, at $x = -0.295m$ (see Figure 1).

The cells upstream of the aerofoil are approximately isotropic, and of size $0.001m$. The aerofoil is meshed using a C-grid, with 250 points on the suction side and 200 points on the pressure side. The cells are clustered at the leading and trailing edges in order to better resolve the sound source regions. A wall-normal first cell height of $y_1^+ \approx 1.6$ is achieved, with ≈ 35 cells used to resolve the boundary layer at the trailing edge. Spanwise slices through the grid at the leading and trailing edges are shown in Figure 2.

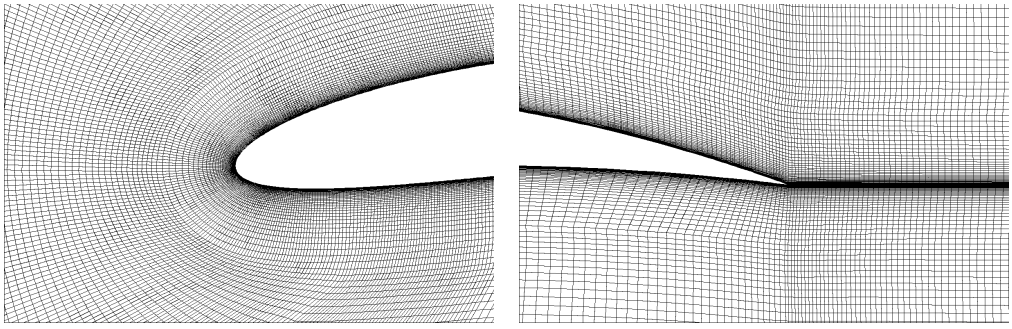

(a) Leading edge (b) Trailing edge

Figure 2: Leading and trailing edge grids for NACA65(12)10 at $Re_c = 2.9 \times 10^5$.

2.4 Computational setup

The turbulent jet is generated using the 'vorton' method of Kornev et al. (2007), which has been implemented into OpenFOAM and made freely available. The turbulence is modelled as homogeneous and *almost* isotropic - since only the streamwise turbulence intensity is known from the experimental measurements, the v' and w' components are estimated as $0.9u'$, based on Comte-Bellot and Corrsin (1966). For the parameters specified, the turbulence generated is divergence free. In order to maintain the stability of the jet shear layer, a small freestream inlet velocity is used, equal to $0.15U_\infty$.

Pressure is set to *zero gradient* (ZG) at the inlet and aerofoil surface, with *fixed value* (FV) at the outlet. Velocity and turbulent kinetic energy are FV zero on the aerofoil, and mixed FV/ZG on the outlet, preventing hydrodynamic reflections. Symmetry planes are used at the top and bottom far field boundarys, while the spanwise sides are periodic. The simulation is initialised from a Reynolds-averaged Navier-Stokes solution, where the residuals for velocity and pressure have reduced to 1×10^{-5}.

A time step $\Delta t = 2 \times 10^{-6} s$ is used, which results in a maximum Courant number, $Co = \Delta t u_i / \Delta x_i \sim 0.65$. The flow is allowed to develop for $\Delta T U_\infty / c = 28$ flow throughs of the domain, after which flow field statistics and acoustic sources are sampled for a further $\Delta T U_\infty / c = 28$ at $\Delta t_{sample} = 1 \times 10^{-5} s$. The simulation duration is approximately 300 hours on 72 23GB processors.

3 Results and Discussion

3.1 Inflow turbulence

The mean velocity and turbulence intensity components are presented in Figure 3, sampled across the jet height at the location $x = -0.2m$, $z = 0.0075m$. The profiles are all approximately uniform across the jet, although the mean velocity does show a $\sim -3\%$ reduction from U_∞ at $y = 0$. The intensities all have similar values, which is surprising considering the v'_{rms} and w'_{rms} components were specified to be smaller than u'_{rms} at the inlet. The mean values between $y = -0.05m$ and $y = 0.05m$ are 2.94% for I_x, and 2.85% for I_y and I_z. Hence all the intensities upstream of the aerofoil are slightly higher that desired. Despite this they do exhibit the characteristics of homogeneous isotropic turbulence.

The power spectra are also seen to be fairly consistent between the three fluctuating components, as shown in Figure 4. The power spectral density (PSD) has been normalised by U_∞^2, with Strouhal number plotted on the abscissa, where $St = fc/U_\infty$. The $-5/3$ power law is included in the Figure to provide an indication of the mesh cut-off frequency. This confirms that the grid is resolving small enough length scales, since a Strouhal number of ~ 11 corresponds to the desired cut-off of $\sim 2\ kHz$.

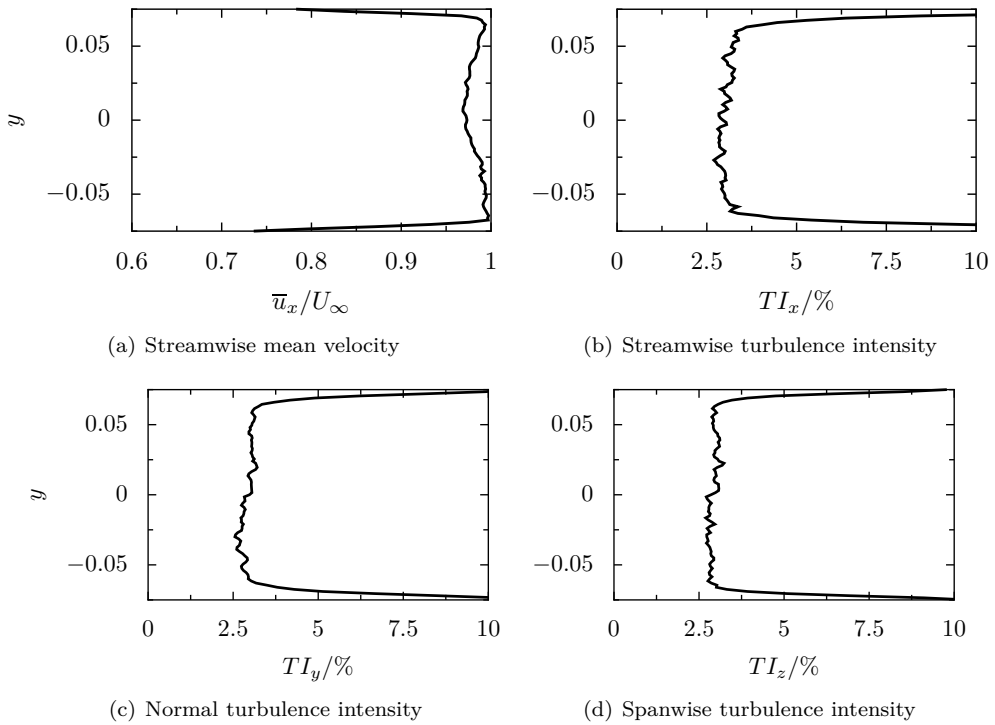

(a) Streamwise mean velocity

(b) Streamwise turbulence intensity

(c) Normal turbulence intensity

(d) Spanwise turbulence intensity

Figure 3: Non-dimensionalised velocity profiles in the jet, sampled across the height of the jet centreline, at $x = -0.2m$.

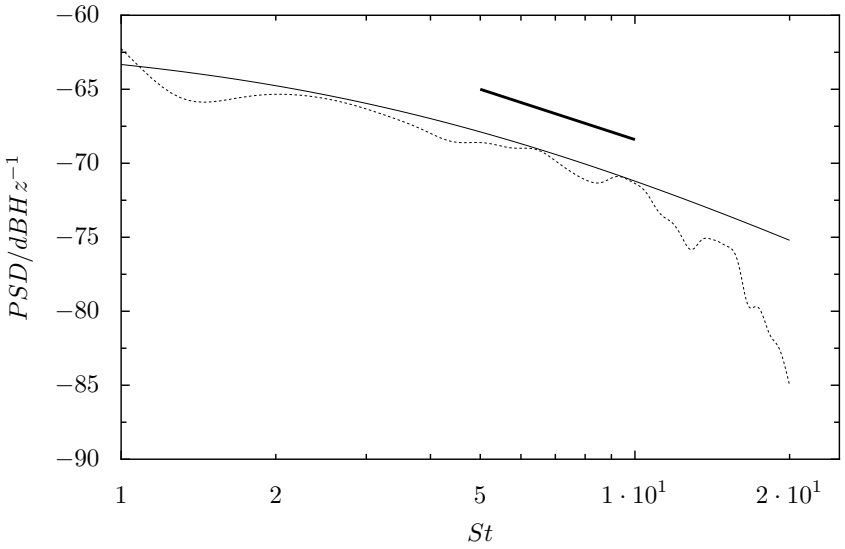

Figure 4: Power spectral density of streamwise velocity fluctuation u', upstream of NACA 651210 leading edge, at $x = -0.2m$: dashed - streamwise; solid - 1-D von Kármán; thick solid - power law with slope $-5/3$.

3.2 Aerodynamic results

The turbulent structures close to the aerofoil surface are visualised in Figure 5 using an iso-surface of $\lambda_2 = 10^7$, coloured by the normalised streamwise velocity. Figure 5 reveals turbulent structures at both the leading and trailing edges, as well as along much of the pressure side of the chord. This has been attributed to a leading edge separation bubble for the 0° angle of attack case (Gruber, 2012). This is corroborated by the chordwise distribution of the pressure coefficent, $C_p = p/0.5\rho U_\infty^2$ where ρ is the fluid density, shown in Figure 6. Figure 6(b) reveals the effect of the pressure side separation bubble on the *rms* surface pressure at approxiamtely $x/c = -0.8$. The unsteady boundary layer structures which lead to trailing edge noise are also noticable for $x/c = -0.4 \to 0$.

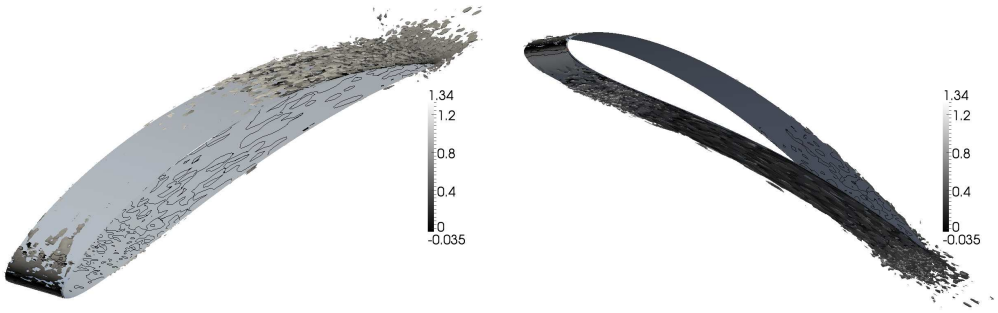

(a) Suction side (b) Pressure side

Figure 5: Iso-surface of $\lambda_2 = 10^7$ coloured by the mean streamwise velocity.

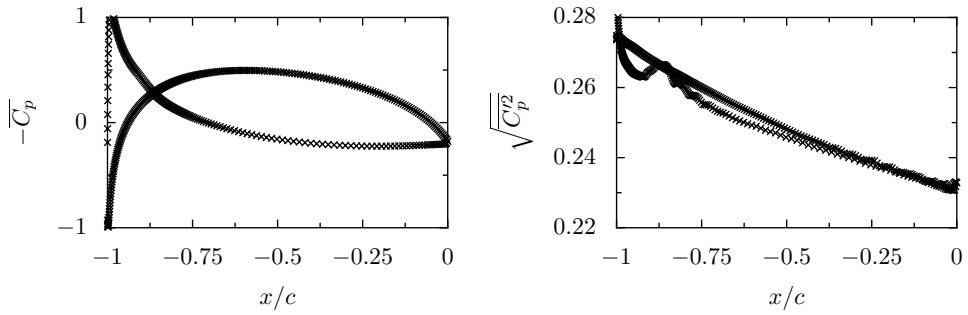

(a) Mean surface pressure coefficient (b) *rms* surface pressure coefficient

Figure 6: Mean and *rms* surface pressure coefficient distribution on NACA65(12)10, sampled at $z/L_z = 0.5$.

3.3 Aeroacoustic results

Figure 7 compares the simulation sound pressure level (SPL) to the experimental data, and the inflow turbulence model of Amiet (1975). This predicts the third-octave SPL based on a von Kármán spectrum for isotropic turbulence as

$$SPL = 10log_{10}\left[\frac{\mathcal{L}sM^5}{2r^2}TI_x^2\frac{\hat{k}_x^3}{(1+\hat{k}_x^2)^{7/3}}\right] + 181.3 \tag{3}$$

where s is the aerofoil span, M the Mach number, r the receiver distance and $\hat{k}_x$ the modified streamwise turbulence wavenumber. This is given by $-\hat{\omega}/u_x$ where $\hat{\omega} = \omega c/2u_x$ and ω is the circular frequency $2\pi f$. The SPL is defined as

$$SPL = 10log_{10}\left(\frac{PSD(f)}{p_{ref}^2}\right) \tag{4}$$

where $p_{ref} = 2 \times 10^{-5}Pa$. In the numerical simulation, the data used to calculate the PSD is the acoustic pressure at the receiver location equivalent to a polar angle of 90°. This has been calculated using the acoustic analogy of Curle (1955), which has been implemented into OpenFOAM by the authors.

The SPL predictions derived from the simulation are corrected for the limited spanwise domain width. To achieve this, the method of Kato et al. (1993) is used, which requires the spanwise coherence length to be estimated. This is given by $L_\gamma = C_c U_c/f$. C_c is a constant determined from the data of Corcos (1963), equal to 0.69 for the 0° angle of attack case presented here. For the frequency range plotted in Figure 7, a correction of $20log(L_\gamma/L_{sim}) + 10log(L_{exp}/L_\gamma)$ is applied to the simulation data.

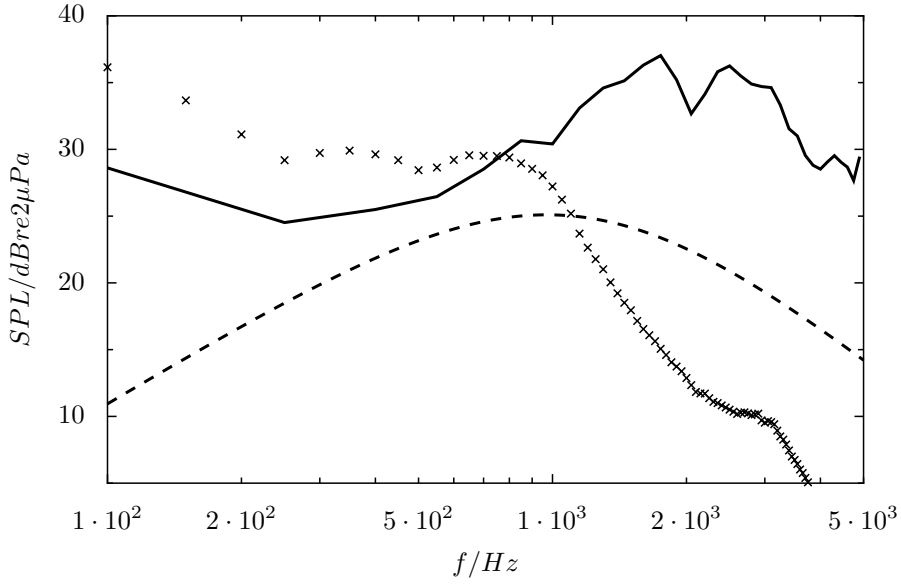

Figure 7: Sound pressure level for NACA 651210 at receiver location $1.22m$ above trailing edge: solid - non-compact Curle's equation; dotted - comapct Curle's equation; dashed - leading edge noise model of Amiet (1975); crosses - experimental data of Gruber (2012).

Figure 7 reveals that the simulation predicts the SPL reasonably well in the range $\sim 400Hz - 1kHz$. However, at higher frequencies the discrepancy between the experimental and simulation result is of the order of 25 dB. This has been attributed to vorticity in the pressure side boundary layer causing a large trailing edge noise source (Deniau et al., 2011). Further work will focus on separating these sources so as to estimate the leading edge noise more accurately. One key observation is the large difference between the experimental and numerical results below $500Hz$. Although the frequencies of the spectral peaks and troughs are correct, the low frequency noise is underpredicted. This suggests that the simulation is not representing the correct range of scales (scales larger than $\mathcal{L}$).

4 Conclusions

The subject of inflow turbulence noise for a fixed aerofoil has been addressed using a viscous flow solver, and the results compared to experimental and empirical predictions. An acoustic analogy approach has been implemented into the code OpenFOAM, thus significantly reducing data post-processing effort when predicting noise.

The IDDES methodology has been shown to provide reasonable prediction of the unsteady aerodynamics that must be captured in order to predict acoustic sources. Use of an inflow turbulence generator has allowed accurate representation of a homogeneous isotropic turbulent inflow. Despite this, the predicted SPL does not closely match experimental data.

Future work will focus on tuning the inflow generator to allow improved noise predictions, and address the problem of inhomogeneous inflow, whereby the turbulence and thus acoustic source strength takes on a spanwise dependency.

5 Acknowledgements

The experimental data was collected by Dr. Gruber as part of the FLOCON project. Gratitude is also expressed to Dr. Richard Sandberg for providing the $k-\omega$ *SST* implementation of IDDES, as well as Evgeny Shchukin for the inflow generator. The authors acknowledge the use of the IRIDIS High Performance Computing Facility, and associated support services at the University of Southampton. Mr Lloyd wishes to acknowledge the financial support of a University of Southampton Postgraduate Scholarship, dstl and QinetiQ.

References

Amiet, R. (1975), 'Acoustic radiation from an airfoil in a turbulent stream', *Journal of Sound and Vibration* **41**(4), 407–420.

Ask, J. and Davidson, L. (2006), The sub-critical flow past a generic side mirror and its impact on sound generation and propagation, number May, pp. 1–20.

Carolus, T. H., Schneider, M. and Reese, H. (2007), 'Axial flow fan broad-band noise and prediction', *Journal of Sound and Vibration* **300**(1-2), 50–70.

Christophe, J., Anthoine, J., Rambaud, P., Schram, C. and Moreau, S. (2007), Prediction of incoming turbulent noise using a combined numerical/semi-empirical method and experimental validation, *in* 'Proceedings of the West-East High Speed Flow Field Conference', 19th-22nd, Moscow.

Comte-Bellot, G. and Corrsin, S. (1966), 'The use of a contraction to improve the isotropy of grid-generated turbulence', *Journal of Fluid Mechanics* **25**(4), 657–682.

Corcos, G. M. (1963), 'The structure of the turbulent pressure field in boundary-layer flows', *Journal of Fluid Mechanics* **18**(03), 353–378.

Curle, N. (1955), 'The influence of solid boundaries upon aerodynamic sound', *Proceedings of the Royal Society A: Mathematical, Physical and Engineering Sciences* **231**(1187), 505–514.

Deniau, H., Dufour, G., Boussuge, J.-F., Polacsek, C. and Moreau, S. (2011), Affordable compressible LES of airfoil-turbulence interaction in a free jet, *in* 'Proceedings of the 17th AIAA/CEAS Aeroacoustics Conference', number June, 5th-8th June, Portland, pp. 1–17.

Devenport, W. J., Staubs, J. K. and Glegg, S. A. (2010), 'Sound radiation from real airfoils in turbulence', *Journal of Sound and Vibration* **329**(17), 3470–3483.

Greschner, B., Thiele, F., Jacob, M. C. and Casalino, D. (2008), 'Prediction of sound generated by a rod-airfoil configuration using EASM DES and the generalised Lighthill/FW-H analogy', *Computers & Fluids* **37**(4), 402–413.

Gruber, M. (2012), Airfoil noise reduction by edge treatments, Ph.D. thesis, University of Southampton.

Kato, C., Iida, A., Takano, Y., Fujita, H. and Ikegawa, M. (1993), Numerical prediction of aerodynamic noise radiated from low Mach number turbulent wake, *in* 'Proceedings of the 31st Aerospace Sciences Meeting and Exhibit', 11th-14th January, Reno, NV.

Kornev, N. V., Kröger, H., Turnow, J. and Hassel, E. (2007), 'Synthesis of artificial turbulent fields with prescribed second-order statistics by the random spots method', *Proceedings in Applied Mathematics and Mechanics* **7**(1), 2100047–2100048.

Michel, U., Eschricht, D., Greschner, B., Knacke, T., Mockett, C. and Thiele, F. (2009), Advanced DES methods and their application to aeroacoustics, *in* S.-H. Peng, P. Doerffer and W. Haase, eds, 'Progress in Hybrid RANS-LES Modelling', Springer-Verlag, pp. 59–76.

Shur, M., Spalart, P. R., Strelets, M. and Travin, A. (2008), 'A hybrid RANS-LES approach with delayed-DES and wall-modelled LES capabilities', *International Journal of Heat and Fluid Flow* **29**(6), 1638–1649.